Microchimica Acta (2021) 188: 107
https://doi.org/10.1007/s00604-020-04676-y

ORIGINAL PAPER

Poly(indole-5-carboxylic acid)/reduced graphene oxide/gold nanoparticles/phage-based electrochemical biosensor for highly specific detection of *Yersinia pseudotuberculosis*

Qiaoli Yang[1] · Sangsang Deng[2,3] · Jingjing Xu[1] · Umer Farooq[1] · Taotao Yang[1] · Wei Chen[1] · Lei Zhou[1] · Meiying Gao[2] · Shenqi Wang[1]

Received: 1 October 2020 / Accepted: 30 November 2020 / Published online: 4 March 2021

Abstract

Yersinia pseudotuberculosis is an enteric bacterium causing yersiniosis in humans. The existing *Yersinia pseudotuberculosis* detection methods are time-consuming, requiring a sample pretreatment step, and are unable to discriminate live/dead cells. The current work reports a phage-based electrochemical biosensor for rapid and specific detection of *Yersinia pseudotuberculosis*. The conductive poly(indole-5-carboxylic acid), reduced graphene oxide, and gold nanoparticles are applied for surface modification of the electrode. They possess ultra-high redox stability and retain 97.7% of current response after performing 50 consecutive cycles of cyclic voltammetry.The specific bacteriophages vB_YepM_ZN18 we isolated from hospital sewage water were immobilized on modified electrodes by Au-NH_2 bond between gold nanoparticles and phages. The biosensor fabricated with nanomaterials and phages were utilized to detect *Yersinia pseudotuberculosis* successfully with detection range of 5.30×10^2 to 1.05×10^7 CFU mL^{-1}, detection limit of 3 CFU mL^{-1}, and assay time of 35 min. Moreover, the biosensor can specifically detect live *Yersinia pseudotuberculosis* without responding to phage-non-host bacteria and dead *Yersinia pseudotuberculosis* cells. These results suggest that the proposed biosensor is a promising tool for the rapid and selective detection of *Yersinia pseudotuberculosis* in food, water, and clinical samples.

Keywords vB_YepM_ZN18 phage · Poly(indole-5-carboxylic acid) · Redox stability · *Yersinia pseudotuberculosis* detection

Introduction

Yersinia pseudotuberculosis (*Y. pseudotuberculosis*) is a Gram-negative bacterium, which is responsible for acute enteric disease along with post-infection complications, including erythema nodosum, reactive arthritis, glomerulonephritis, Reiter's syndrome, sepsis, and myocarditis [1]. Symptoms of such illness are often clinically indistinguishable from those of acute appendicitis, thus possibly leading to unnecessary appendectomies [2]. Therefore, early-stage detection of this bacterium is important to avoid probable improper treatment of already infected people. Conventional plate-culture and colony-count detection method for *Y. pseudotuberculosis* is reliable, but it is laborious and time-consuming [3]. Several modern detection techniques have been reported, such as enzyme-linked immunosorbent assays (ELISA) [1], polymerase chain reaction (PCR), and PCR derivatives (e.g., real-time PCR, multiplex PCR, or loop-mediated isothermal amplification) [4–6]. Although these techniques are sensitive and rapid, there are still some disadvantages limiting their capability of onsite detection, such as the requirement of professional staff, expensive reagents, and the possibility of obtaining false positive results [7–9]. Thus, the development of advanced, simple, and rapid methods for

Qiaoli Yang and Sangsang Deng contributed equally to this work.

✉ Meiying Gao
mygao@wh.iov.cn

✉ Shenqi Wang
shenqiwang131@hust.edu.cn

[1] Advanced Biomaterials & Tissue Engineering Centre, College of Life Science and Technology, Huazhong University of Science and Technology, Wuhan 430074, People's Republic of China

[2] Wuhan Institute of Virology, Chinese Academy of Sciences, Wuhan 430071, People's Republic of China

[3] University of Chinese Academy of Sciences, Beijing 100039, People's Republic of China

Y. pseudotuberculosis detection is highly required and crucial to overcome such limitations.

Recently, electrochemical biosensors are attention-grabbing because of their excellent sensitivity, low cost, rapid analysis, and easy for miniaturization [10]. However, nucleic acid or antibodies-based biosensors for bacterial detection cannot discriminate live and dead cells, potentially result in a false-positive/-negative outcome [11]. Additionally, the sensitivity of such bio-recognition elements to extreme temperature, pH, and other environmental conditions are limiting their practical application [12]. On the other hand, bacteriophages are exciting recognition elements in biosensors development because of their high specificity toward target bacterium, tolerance to extreme temperature and pH, ability to discriminate live/dead bacteria, and cost-effective and simple production in bulk [13]. To date, many phage-based biosensors have been reported for the detection of *Escherichia coli*, *Salmonella*, *Staphylococcus aureus*, and other common pathogenic bacteria [3].

Various types of redox-active materials have been reported as electronic media in the development of electrochemical biosensors, such as ferrocene, Prussian blue, and methylene blue [14–16]. Such redox-active materials suffer from low conductivity and poor stability [17]. The development of electrochemical biosensor with highly stable redox-signal is still challenging. Application of the poly(indole-5-carboxylic acid) (PI–5–CA) is receiving immense interest in the field of electrochemistry owing to its eminent properties such as abundant functional groups, great electrical conductivity, and high redox activity [18]. However, utilization of PI–5–CA in electrochemical biosensors is reported in the literature mostly for immobilization applications, only a few articles report its redox-active applications [19, 20]. Therefore, the excellent property of PI–5–CA was utilized in the development of electrochemical biosensor, alternatively boosting the biosensor performance. In addition to the PI–5–CA, the incorporation of reduced graphene oxide (rGO) and gold nanoparticles (AuNPs) can further improve the redox stability as well as electrical conductivity due to its fast electron transfer rate and electrocatalytic activity [16, 21].

The current study reports the development of a PI–5–CA/rGO/AuNPs/phage-based electrochemical biosensor for specific detection of *Y. pseudotuberculosis*. Firstly, we collected the hospital sewage water and isolated specific phages as bio-recognition element for the fabrication of biosensor. Then we synthesized the PI–5–CA/rGO/AuNPs material for electrode modification. The exact composition of the material was demonstrated by FTIR, Raman, and EDX tests. The redox stability and conductivity of material were investigated by electrochemical characterization. Subsequently, the phage was immobilized on modified electrodes. The density of immobilized phages was determined through fluorescent observations. The feasibility and detection principle of the prepared biosensor was expounded by SEM, DPV, and EIS analysis. Finally, our phage-based biosensor was utilized for real samples detection and its reliability was confirmed by comparing with the conventional method.

Materials and methods

Reagents

Indole-5-carboxylic acid (I–5–CA) was purchased from Shanghai Vita Chemical Regent Co., Ltd. (Shanghai, China). Graphene oxide (GO) was purchased from Nanjing Xian Feng Nanomaterials Technology Co., Ltd. (Nanjing, China). Tetrachloroauric acid trihydrate ($HAuCl_4{\cdot}3H_2O$) was purchased from Aladdin Chemistry Co., Ltd. (Shanghai, China). Bovine serum albumin (BSA) was purchased from Sigma-Aldrich (USA). Ethanol, ammonium persulfate (APS), H_2SO_4, L-ascorbic acid, and trisodium citrate were purchased from Sinopharm Chemical Co. Ltd. (Shanghai, China). Phosphate buffer (PBS) was prepared with 1:1 (0.1 M) NaH_2PO_4 and Na_2HPO_4 with different pH values.

Bacterial culture

Y. pseudotuberculosis (kindly provided by Prof. Meiying Gao's lab) was grown in 5 mL of Luria-Bertani (LB) medium in a shaking incubator at 37 °C for 6 h. Then the bacterial culture was centrifuged at 4000 g for 10 min to completely remove the media, and the pellet was resuspended in PBS. The concentration of bacteria was evaluated by agar plate count method and expressed in colony-forming units per milliliter (CFU mL^{-1}). All details about other bacterial strains used in the current study were described in the Supplementary Information file.

Phage isolation, propagation, and characterization

Y. pseudotuberculosis specific phage was isolated from hospital sewage water (Zhongnan Hospital of Wuhan University, Wuhan, China) following the basic protocol of lambda phage isolation (Scheme S1). Briefly, the sewage water sample was centrifuged at 4000 g for 10 min, followed by filtration of the supernatant through a 0.22 μm syringe-driven filter. Next, 0.2 mL filtrate was added into 5 mL of *Y. pseudotuberculosis* culture at log phase in 10 mL of 3 × LB, and followed by incubation at 37 °C for 24 h. The incubated culture was again centrifuged at 4000 g for 10 min and filtered through a 0.22 μm filter to remove bacteria. Subsequently, the filtrate was serially diluted and incubated with logarithmic phase *Y. pseudotuberculosis* for 10 min; double agar overlay plaque assay was carried out for plaque assay. Single plaque of phage was selected and repeated double agar overlay plaque assay at least six times in order to purify the phage. Furthermore, the isolated bacteriophage was

amplified using double agar overlay plaque assay. Briefly, 200 μL of *Y. pseudotuberculosis* at log phase and 100 μL of phage (10^4~10^5 PFU mL^{-1}) were added to molten soft agar (LB containing 0.5% agarose), poured onto LB plates, and overnight incubated at 37 °C. SM buffer (3 mL) was then added to the plates, shaking horizontally for 2 h. Then the solution was collected to centrifuge and filter in order to remove bacteria and debris. Finally, the phage titer was measured using plaque assay and expressed in PFU mL^{-1}.

The genome extraction from bacteriophage was performed according to the method described by Santos [22] with some modifications. The Illumina Hiseq 2500 system (Illumina, San Diego, CA, USA) was used to sequence genomic DNA. The genome was assembled with the software SPAdes-3.5.0. Open reading frames (ORFs) and tRNA were predicted with RAST (http://rast.nmpdr.org/rast.cgi). The morphology of phage was characterized by a transmission electron microscope (TEM) (HT7700, HITACHI, Japan). The phage samples were prepared by absorbing the phage on copper-Formvar-carbon grids (Ted Pella, Inc.) for 10 min, followed by negative staining for 2 min with 4% phosphotungstate (pH = 6.8). The grids with adsorbed phages were air-dried before examining under the microscope.

Fabrication of PI–5–CA/rGO/AuNPs/phage-based electrode

To develop a phage-based working electrode, surface of the glassy carbon electrode (GCE) was polished twice with alumina powder of 0.3 μm and then with 0.05 μm, followed by ultrasonic cleaning in deionized water and ethanol. The preparation of PI–5–CA/rGO/AuNPs materials was described in the Supplementary Information file. Then PI–5–CA/rGO/AuNPs materials (8 μL) was carefully dropped on the electrode and dried at room temperature, followed by washing with deionized water to remove unfixed materials from the surface of the electrode. Then 8 μL of isolated phage vB_YepM_ZN18 (10^{10} PFU mL^{-1}) was incubated on PI–5–CA/rGO/AuNPs-modified electrode at 37 °C for 2 h, followed by washing with deionized water to remove any unbound phages. Subsequently, BSA (1 mg mL^{-1}, 8 μL) was added on the surface of the modified electrode and allowed to incubate at 37 °C for 30 min to block the nonspecific binding sites, followed by washing with deionized water to remove free BSA. Thus, the obtained phage-based electrode was stored at 4 °C for subsequent bacterial detection.

Characterization of the modified electrode

The morphology of the developed PI–5–CA/rGO/AuNPs/phage-based electrode was characterized under a field emission scanning electron microscope (FE-SEM) (Nova NanoSEM 450, FEI, Netherlands), while variations in functional groups were characterized by Fourier transform infrared spectrometer (FTIR) (VERTEX 70, Bruker, Germany). The constituent elements of the composition were studied by the X-ray photoelectron spectroscopy (XPS) (AXIS-ULTRA DLD-600 W, Shimadzu, Japan). The structural features of the composite were studied by an x'pert3 powder diffraction (XRD) instrument (PANalytical B.V., Netherlands). For fluorescent characterization of phages, 100 μL of 10^{10} PFU mL^{-1} of phages were stained with 5× SYBR gold (fluorescent nucleic acid stain) for 20 min [23]. Prior to fluorescent observations, any free dye on phage particles were removed by diluting and centrifuging across a 100 kDa (EDM Millipore, UFC 910008) filter four times. After 4-step of centrifugation, the phage was resuspended in saline to the original volume. The stained phages were then immobilized on PI–5–CA/rGO/AuNPs modified indium tin oxide (ITO) electrode and observed under confocal microscope (FV1000 IX81, Olympus, Japan). The Electrochemical workstation CHI630E (Shanghai Chenhua Instrument, China) was used for electrochemical characterization in a typical three-electrode cell. The cell contained a counter electrode (platinum 5 mm × 5 mm), a reference electrode (Ag/AgCl electrode), and a bare GCE (Φ = 3 mm) as the working electrode. The modified electrode was characterized electrochemically by cyclic voltammetry (CV), differential pulse voltammetry (DPV), and electrochemical impedance spectroscopy (EIS) analysis. At potential range from − 0.3 to 0.7 V (vs. Ag/AgCl), the CV analysis was recorded at a scan rate of 100 mV s^{-1} and DPV analysis was recorded at the amplitude of 50 mV and with a pulse period of 0.2 s. EIS analyses were performed at room temperature in 5.0 mM $[KFe(CN)_6]^{3-/4-}$ (1:1) containing 0.1 M KCl.

Electrochemical detection of *Y. pseudotuberculosis*

For electrochemical detection of *Y. pseudotuberculosis*, 6 μL of bacterial cultures with different cell densities (5.30×10^2 CFU mL^{-1}, 6.40×10^3 CFU mL^{-1}, 1.80×10^5 CFU mL^{-1}, 7.90×10^5 CFU mL^{-1}, 5.10×10^6 CFU mL^{-1}, 1.05×10^7 CFU mL^{-1}) were incubated on PI–5–CA/rGO/AuNPs/phage-based biosensor at 37 °C for 30 min. The PI–5–CA/rGO/AuNPs/phage-based electrodes were washed with PBS to remove any unbound bacteria. Finally, DPV analysis was recorded at potential range from − 0.3 to 0.7 V (vs. Ag/AgCl) in PBS (0.1 M, pH 6.0).

Specificity, live/dead cells discrimination, reproducibility, and storage stability

The specificity of our proposed biosensor was determined against *Y. pseudotuberculosis* and other non-host bacteria like. Briefly, *Y. pseudotuberculosis* and *Yersinia pekkanenii*, *E. coli* O157:H7, *Yersinia enterocolitica*, *S. aureus* at same cell

density (3.00×10^6 CFU mL^{-1}) were incubated on modified electrodes for 30 min and DPV measures were performed. As the control, PBS (no bacteria) and a mixture of all host and non-host bacteria were also detected by the same condition. Further, the ability of our proposed biosensor to detect live *Y. pseudotuberculosis* cells in a mixture of live/dead *Y. pseudotuberculosis* cells was studied by the DPV measures. The concentration of live bacterial cells can be measured by plate count method (3.30×10^5 CFU mL^{-1}) and the same concentration of dead bacterial cells was obtained by sterilization of live bacterial cells (3.30×10^5 CFU mL^{-1}) at 121 °C for 25 min. The dead and live bacterial cells at same concentration were mixed (1:1) and applied for detection.

The storage stability of this biosensor was assessed within 4 weeks; the PI–5–CA/rGO/AuNPs/phage-based biosensor was stored at 4 °C and measured by DPV every week. Additionally, the reproducibility of the PI–5–CA/rGO/AuNPs/phage-based biosensor was evaluated by DPV measurement with *Y. pseudotuberculosis* (8.00×10^5 CFU mL^{-1}) by preparing seven separately modified electrodes.

Analysis of real samples

The practical application of our proposed phage-based biosensor was evaluated to detect *Y. pseudotuberculosis* in river water samples (collected from East Lake, Wuhan, China). For analysis, the river water samples were inoculated with different volume of bacterial culture. Then the cell density of bacteria was analyzed by the plate count method and our proposed phage-based biosensor.

Results and discussion

In this study, a PI–5–CA/rGO/AuNPs/phage-based biosensor was proposed for *Y. pseudotuberculosis* detection. The step-by-step fabrication of biosensor with PI–5–CA/rGO/AuNPs materials and phages, and application for *Y. pseudotuberculosis* detection are presented in Scheme 1.

Morphology characterization and genome analysis of isolated phage

The isolated bacteriophage (vB_YepM_ZN18) from hospital sewage water produced clear plaques on the plate of *Y. pseudotuberculosis* (Fig. 1a). It demonstrates that the phage is a virulent bacteriophage that lysed *Y. pseudotuberculosis* and generated the progeny phages. The average particle size of phages was estimated by randomly selecting 20 particles from the TEM micrograph. The results reveal a head of 106.1 ± 3.6 nm and a contractile tail of 110.4 ± 2.6 nm (Fig. 1b).

The host range of phage vB_YepM_ZN18 is confirmed by infecting different bacteria. It is one of the defining biological characteristics to confirm phage specificity toward a particular bacterium. As shown in Table S1, the phage vB_YepM_ZN18 do not show infectivity to non-host bacteria but infect *Y. pseudotuberculosis* specifically. Compared to the phage PY 100 [24], PST [25] with broad host range toward *Yersinia* species, the isolated phage vB_YepM_ZN18 from hospital sewage water shows great specificity toward *Y. pseudotuberculosis*. It is appropriate for the development of phage-based biosensors to specifically detect *Y. pseudotuberculosis*.

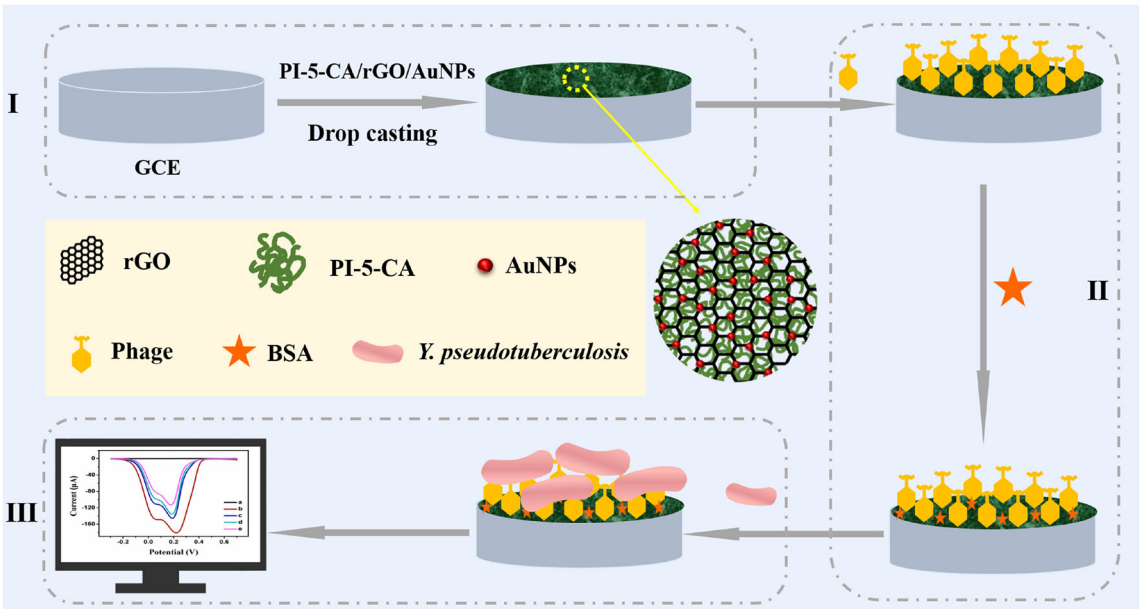

Scheme 1 Schematic illustration of (I) glassy carbon electrode (GCE) modification with PI–5–CA/rGO/AuNPs materials, subsequent (II) immobilization of isolated phage to develop PI–5–CA/rGO/AuNPs/phage-based bio-electrode and (III) application for *Y. pseudotuberculosis* detection by electrochemical analysis.

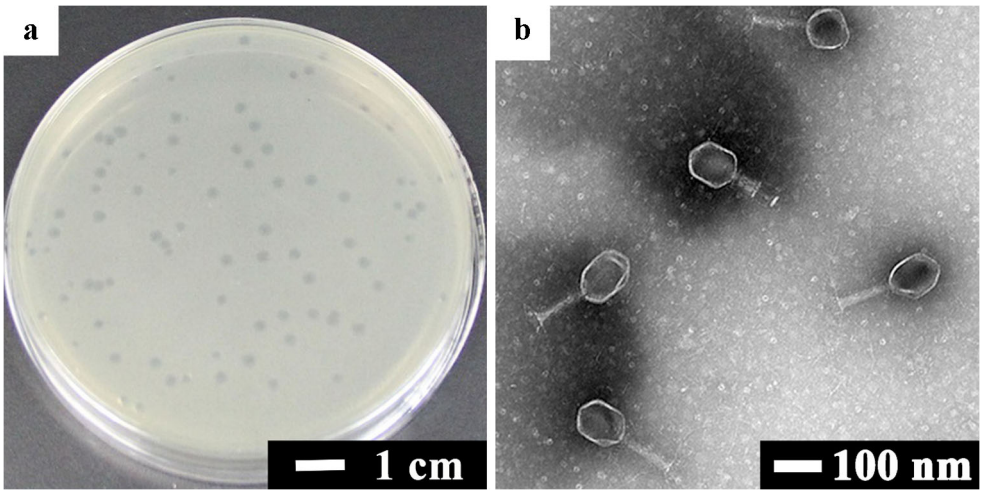

Fig. 1 Plaques observation and morphology analysis of isolated phage vB_YepM_ZN18. **a** Photograph of plaques produced by isolated phage, and **b** the morphology of isolated phage by TEM

The genome of phage vB_YepM_ZN18 was sequenced by Illumina Hiseq 2500 system and assembled with SPAdes-3.5.0. The genome analysis reveals that it consists of 167,856 bp of dsDNA with a G + C content of 35.4%. This phage genome is more similar to *Escherichia coli* phage vB_EcoM_ACG-C40, sharing 96.23% nucleotide sequence identities. A total of 275 ORFs were identified on the isolated phage genome, 264 ORFs encode proteins and 11 ORFs encode tRNA. Most ORFs are reverse transcribed, while only 43 ORFs are forward transcribed. Sequence alignment of 264 ORFs revealed that 144 ORFs had significantly similar genes in the database. The complete genome sequence of phage vB_YepM_ZN18 has been deposited in GenBank under accession no. MN716856.

The characterization of PI–5–CA/rGO/AuNPs materials and immobilized phages on the modified electrode

The PI–5–CA/rGO/AuNPs materials was synthesized and characterized by FTIR Raman, and XPS. The PI–5–CA was obtained by the polymerization of I–5–CA. The variation in functional groups is confirmed by FTIR analysis. As shown in Fig. 2a, there is an apparent decline in peak intensity of PI–5–CA compared to the spectra of I–5–CA, attributed to the

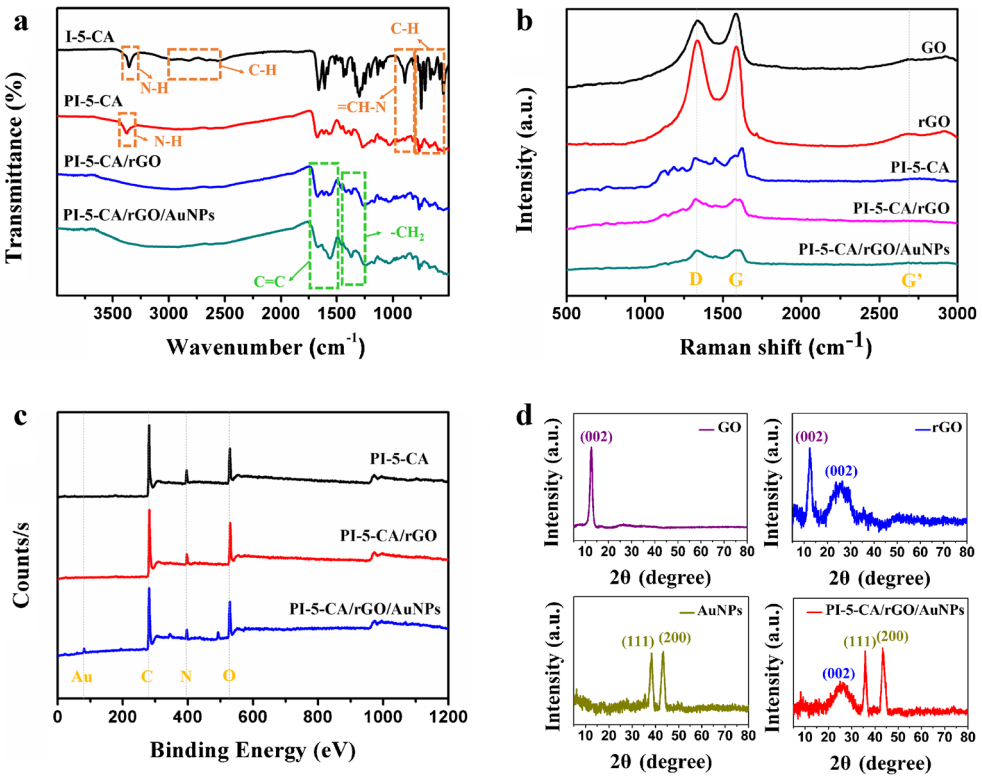

Fig. 2 Characterization of PI–5–CA/rGO/AuNPs materials: **a** FTIR of I–5–CA, PI–5–CA, PI–5–CA/rGO, and PI–5–CA/rGO/AuNPs; **b** Raman spectra of GO, rGO, PI–5–CA, PI–5–CA/rGO, and PI–5–CA/rGO/AuNPs; **c** XPS of PI–5–CA, PI–5–CA/rGO, and PI–5–CA/rGO/AuNPs; **d** XRD of GO, rGO, AuNPs, and PI–5–CA/rGO/AuNPs

distribution of polymers' wide conjugated chain length [26]. As shown in the spectra of both I–5–CA monomer and PI–5–CA polymer, the peaks in the range of 710 cm^{-1} and 825 cm^{-1} are ascribed to the three C–H deformation vibration on the benzene ring, suggesting that the polymerization of I–5–CA maybe happened at the pyrrole ring [27]. For I–5–CA, the stretching vibration of =CH–N appeared at 893 cm^{-1}, whereas such peak disappeared in the spectra of PI–5–CA [28]. The peaks around 2531–2985 cm^{-1} in the spectra of I–5–CA and PI–5–CA signify the presence of carboxyl groups. The broad peaks in the spectra of both I–5–CA and PI–5–CA at 3360 cm^{-1} prove that N–H stretching vibration of the pyrrole ring still existed on the polymers. These results reveal that the polymerization of I–5–CA monomer might occur at the positions 2 and 3 of the pyrrole ring as stated elsewhere [20]. Furthermore, the FT-IR analysis of PI–5–CA/rGO composite show a shift in C=C bond compared with the spectrum of PI–5–CA. It can be assigned to the π-π interaction between PI–5–CA and rGO [20]. Additionally, the presence of AuNPs mixed with PI–5–CA/rGO composite enhance the vibration frequency of –C=C (at 1558 cm^{-1}) and $–CH_2$ (the absorption peak at 1471 cm^{-1}), suggesting AuNPs are interacting with the PI–5–CA/rGO composite [29].

The presence of rGO in the PI–5–CA/rGO/AuNPs materials was proved by Raman analysis. In the Raman spectra of the GO, there are typical G band (the E2g mode of sp2 carbon atoms) and D band (the symmetry A1g mode) which reveals the change of the electronic conjugation state. As described in Fig. 2b, the ratio of D/G intensity increased significantly along with the reduction which is consistent with previous report [30], indicating the reduction of GO had happened. Compared to the ratio of D/G intensity in GO, that ratio of the PI–5–CA/rGO and PI–5–CA/rGO/AuNPs are found to be higher, confirming the deoxygenation during the synthesis process of the composite. X-ray photoelectron spectroscopy (XPS) spectra are also used for further analysis the composition. Figure 2c displays the index peaks of PI–5–CA/rGO/AuNPs, which are related to the elements C, N, O, Au. The constituent elements of the PI–5–CA/rGO/AuNPs composite, especially the existence of Au, are confirmed through the comparison of different materials.

The crystallinity of PI–5–CA/rGO/AuNPs was studied by an X-ray diffraction (XRD) technique, and corresponding XRD pattern was shown in Fig. 2d. After the reduction, the sharp XRD peak of GO (at $2\theta = 12.6°$) become weaker, but a new broad diffraction peak (at $2\theta = 25.4°$) appeared, which is closer to the typical (002) diffraction peak of graphite (at $2\theta = 26.1°$). This result further supports the incompletion reduction of GO by L-AA [31]. The distinct peaks at $2\theta = 38.1$ and 44.3 corresponded to standard Bragg reflections (111), (200) of face center cubic lattice which is typical XRD pattern of pure Au nanocrystals [32].

Furthermore, bacteriophages were immobilized on modified electrodes for the fabrication of biosensor. To visualize densities of immobilized bacteriophage on the electrode surface, phages were stained with SYBR gold dye [23]. As the control, the confocal image of PI–5–CA/rGO/AuNPs with and without phage immobilization in the absence of SYBR gold dye show no fluorescence as expected (Fig. S1A-B). On the other hand, phage particles labeled with SYBR gold dye showed some fluorescent dots (Fig. S1C), suggesting that fluorescence is generated from the reaction of dye with the nucleic acid of the phages, neither PI–5–CA/rGO/AuNPs materials nor phages. Figure 3a, b displays the densities of

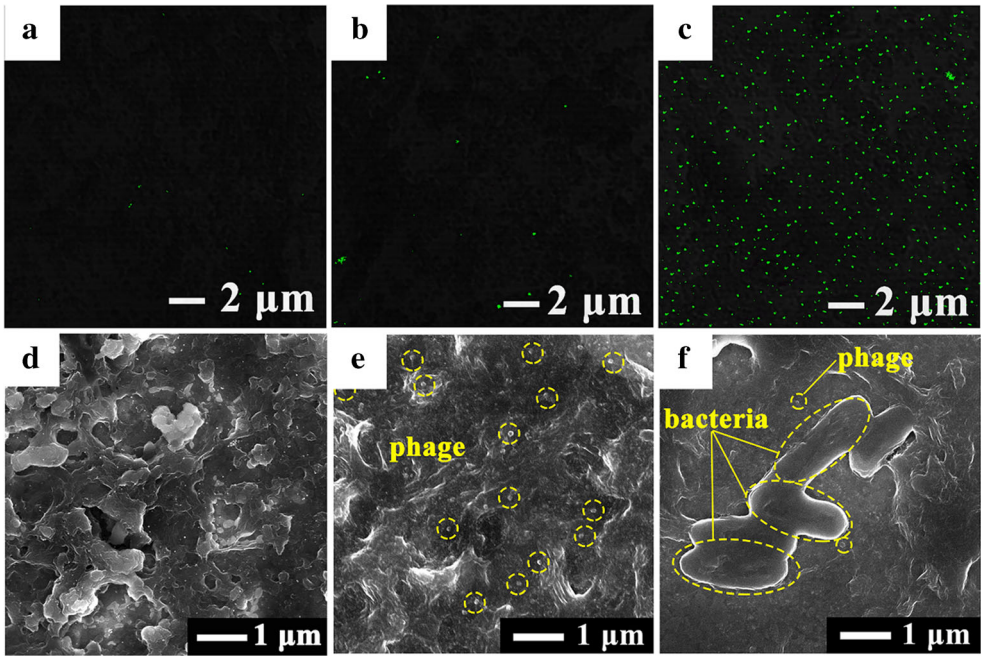

Fig. 3 Fluorescent observation of immobilized phages' density on different modified electrodes, and morphological observation of the materials, phage immobilization, and bacterial capture. The phages were stained with SYBR gold (a fluorescent nucleic acid stain). The confocal microscopy images of labeled phage particles immobilized on ITO electrode which modified with **a** PI–5–CA, **b** PI–5–CA/rGO, and **c** PI–5–CA/rGO/AuNPs. FE-SEM characterization of **d** PI–5–CA/rGO/AuNPs/GCE, **e** phage immobilized PI–5–CA/rGO/AuNPs/GCE, and **f** following bacterial capture

immobilized phages on the surface of electrodes modified with PI–5–CA, PI–5–CA/rGO, and PI–5–CA/rGO/AuNPs materials, respectively. The results in PI–5–CA (Fig. 3a) and PI–5–CA/rGO materials (Fig. 3b) immobilize few phages, whereas a greater density of immobilized phage particles is observed in the PI–5–CA/rGO/AuNPs materials (Fig. 3c), suggesting that AuNPs facilitate phage immobilization. From Fig. 3c, the calculated densities by ImageJ software were 2.51 ± 0.4 phage particles.μm^{-2}. These results demonstrated that PI–5–CA/rGO/AuNPs supported the phage immobilization, possibly through Au-NH_2 bond between AuNPs and vB_YepM_ZN18 phages as reported [33]. Most phages have a negatively charged capsid (head) and positively charged tail fibers [23, 34]. The charge difference between head and tail fibers of the phage could be utilized for immobilizing phage on electrode surface using electrostatic interaction. To confirm the loss/retention of phage lytic activity after being immobilized, the disc diffusion method was used to study the immobilized phages. The results in Fig. S2 reveal the immobilized phage retained the lytic activity to infect *Y. pseudotuberculosis* and formed clear plaques on the lawn of *Y. pseudotuberculosis*.

The structural morphologies of PI–5–CA/rGO/AuNPs, PI–5–CA/rGO/AuNPs/phage, and PI–5–CA/rGO/AuNPs/phage/bacteria on ITO glass slides were observed by SEM. The SEM micrograph of PI–5–CA/rGO/AuNPs materials reveals a porous structure, with many AuNPs-like nanoparticles (~20 nm) on the surface (Fig. 3d). This configuration of nanomaterial is believed to offer a large surface area and promising microenvironment for easy immobilization of biomolecules [20]. Figure 3e shows immobilization of phage-like particles on PI–5–CA/rGO/AuNPs electrode. The diameter of particles is about 220 nm, suggesting the head and the less obvious tail of phage [35]. The potential of immobilized bacteriophage particles to capture bacterial cells is demonstrated in Fig. 3f**.** The results showed that the phage particles retain the bacterial recognition capability followed by capture. Thus, the activity of phage particles was not affected after being immobilized on PI–5–CA/rGO/AuNPs-modified electrode.

Electrochemical characterization of fabrication process of the phage-based biosensor

The electrochemical role of each component in the fabrication process of PI–5–CA /rGO/AuNPs-based electrode was characterized by CV measurement. As shown in Fig. 4a, CV curves of bare GCE, PI–5–CA/GCE, PI–5–CA/rGO/GCE, PI–5–CA/AuNPs/GCE, rGO/AuNPs/GCE, and PI–5–CA/

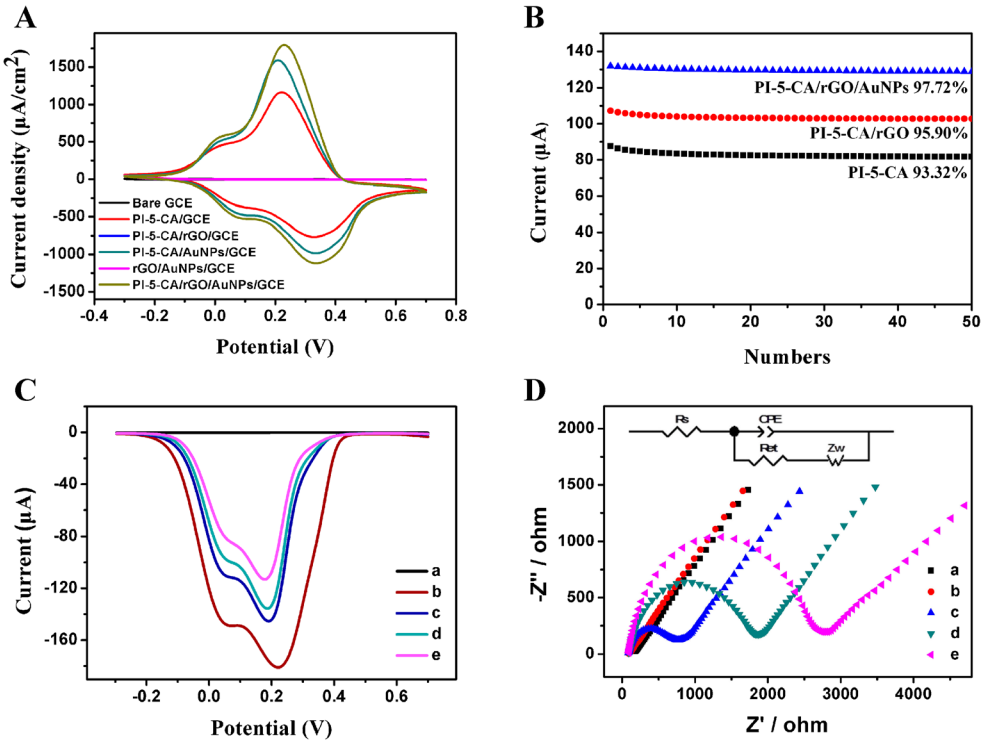

Fig. 4 Electrochemical characterization of different modified electrodes, and the current and impedance changes during the fabrication process of biosensor: **a** The current density measurements of bare GCE, GCE/PI–5–CA, GCE/PI–5–CA/rGO, GCE/PI–5–CA/AuNPs, GCE/rGO/AuNPs, GCE/PI–5–CA/rGO/AuNPs at −0.3~0.7 V in PBS (0.1 M, pH 6.0), scan rate: 100 mV s^{-1} (Ag/AgCl electrode as the reference electrode); **b** Redox signal stability of the different modified electrode after 50 cycles of continuous CV measurement; **c** DPV measurements at −0.3~0.7 V in PBS (0.1 M, pH 6.0); and **d** electrochemical impedance spectra in 5.0 mM $[KFe(CN)_6]^{3-/4-}$ (1:1) containing 0.1 M KCl of: (a) bare GCE, (b) GCE/PI–5–CA/rGO/AuNPs, (c) GCE/PI–5–CA/rGO/AuNPs/phage, (d) GCE/PI–5–CA/rGO/AuNPs/phage/BSA, (e) GCE/PI–5–CA/rGO/AuNPs/phage/BSA/bacteria. The frequency range was 0.1–10,000 Hz with signal amplitude of 5 mV

rGO/AuNPs/GCE were recorded in 0.1 M PBS (pH 6.0). No obvious redox peak current was observed for bare GCE and rGO/AuNPs/GCE, while obvious redox peak was observed after electrode modification with PI–5–CA, suggesting the electrochemical redox activity of PI–5–CA as reported elsewhere [36]. Moreover, a rise in peak currents was observed after incorporation of rGO on the PI–5–CA–modified electrode. It reveals the successful fabrication of electrode surface with rGO promote the electron transfer and enhance the effective electrode surface area [37]. Graphene has fast electron transfer rate and electrocatalytic activity which could be attributed to the high density of electronic states, abundant defective site, and oxygen containing groups at the edge of graphene [19]. Additionally, a rise in peak currents was observed on the PI–5–CA/AuNPs-modified electrode that revealed AuNPs, ultimately facilitated electron transfer [38, 39]. Furthermore, CV analysis of PI–5–CA/rGO/AuNPs-modified electrode revealed a further increase in the peak current, suggesting incorporation of rGO and AuNPs improved the electron transfer and electrocatalytic activity together which enhance the current responses [40].

The pH of electrolyte greatly affects the electrochemical performance of the modified electrode, so it is necessary to confirm the optimal pH of electrolyte for subsequent electrochemical measurements. By the analysis of current response and stability, PBS (pH 6.0) is chosen as the optimal electrolyte for subsequent electrochemical measurements (Fig. S3). Also, the relationship between the current response and scan rate was investigated and the result (Fig. S4) shows that the involved electrochemical reaction is an adsorption-controlled process [41]. Meanwhile, the signal stability of PI–5–CA, PI–5–CA/rGO and PI–5–CA/rGO/AuNPs-modified electrodes was studied by performing 50 consecutive cycles of CVs. The percentage of retained current response is 93.3%, 95.9%, and 97.7% for PI–5–CA, PI–5–CA/rGO, and PI–5–CA/rGO/AuNPs-modified electrodes respectively, confirming the enhanced stability (Fig. 4b). Compared with other reports about redox-active materials used for electrochemical biosensor [15, 16], PI–5–CA/rGO/AuNPs materials showed higher redox activity and stability, suggesting its promising role in development of phage-based electrochemical biosensor.

The detection principle of our prepared biosensor is that vB_YepM_ZN18 phage as a bio-recognition element can capture *Y. pseudotuberculosis* specifically. Due to the nonconductive bacteria that hinder the electrons transfer, the current responses decrease [33], and the variations before and after capture events were recorded by the electrochemical workstation. In addition, the PI–5–CA/rGO/AuNPs material is applied for modified electrodes for amplifying current response. The fabrication process of the phage-based biosensor was characterized by DPV measurement. As shown in Fig. 4c, DPV curves of bare GCE, GCE/PI–5–CA/rGO/AuNPs, GCE/PI–5–CA/rGO/AuNPs/phage, GCE/PI–5–CA/rGO/AuNPs/phage/BSA, and GCE/PI–5–CA/rGO/AuNPs/phage/BSA/bacteria were recorded in 0.1 M PBS (pH 6.0). No peak current is observed for bare GCE while PI–5–CA/rGO/AuNPs show a significant current response. The two peaks in DPV curve could be attributed to two electrochemical redox processes associated with the PI–5–CA. The first process occurs over a broad potential range of 0.02~0.07 V. The second process, which appears at higher potentials around 0.17 V, exhibits the most sharply defined voltammetric peaks [42]. This result reveals an enhanced electron transfer which is attributed to strong redox activity and outstanding conductivity of PI–5–CA/rGO/AuNPs materials. When incubating phage on PI–5–CA/rGO/AuNPs-modified electrode, the obvious decrease of the current response is observed. The possible explanation is that nonconductive phage hinders electron transfer, demonstrating that phage was immobilized on the modified electrode successfully [43]. The immobilization might be realized by connecting AuNPs and the vB_YepM_ZN18 phages through Au-NH_2 bond [44]. When adding BSA on the electrode for blocking the non-specific sites of the modified electrode, an additional decrease current response is observed due to the nonconductive behavior of BSA [41]. Finally, after the phage-based biosensor was incubated with *Y. pseudotuberculosis*, a further decrease in current response was recorded, confirming the specific capture of phage for *Y. pseudotuberculosis* [45]. These results confirm the feasibility of our proposed biosensor for *Y. pseudotuberculosis* detection.

EIS technology is also used to reflect the stepwise fabrication of the electrode surface. To obtain impedance values, EIS data is fitted with the equivalent circuit model (the inset in Fig. 4d). The circuit consists of electron transfer resistance (Ret), Warburg impedance (Zw), electrolyte resistance (Rs), and constant phase element (CPE). As Ret values vary obviously when different materials are modified on the electrode surface, it is a sensitive indicator that can be used to reflect the modification events happening on the surface of the work electrode. These nonconductive materials (such as phages, BSA, bacteria) hamper electron transfer, causing an increase of Ret value. As shown in Fig. 4d, a little Ret (174.4 Ω) demonstrates that bare electrodes have good electron transfer ability (Curve a). After PI–5–CA/rGO/AuNPs materials are used to modify electrode, almost a straight line is observed owing to the excellent conductivity of PI–5–CA /rGO/AuNPs materials (Curve b). After phages were immobilized on PI–5–CA /rGO/AuNPs-modified electrode, the Ret (771.5 Ω) is increased (curve c). The Ret (1852.0 Ω) is increased when the uncombined sites on the PI–5–CA/rGO/AuNPs/phage-based electrode surface are blocked by BSA (curve d). Continuous increasing of the Ret (2769.0 Ω) is observed after capturing *Y. pseudotuberculosis* (curve e). In short, the value of impedance increases gradually with the stepwise modification of materials on the electrode surface, and this consists with the variations of current responses measured by DPV. These results prove that phage-based electrochemical biosensor is constructed successfully.

Y. pseudotuberculosis detection with phage-based biosensor

To optimize the performance of the phage-based biosensor, the phage incubation time and the response time for detection are the important factors to be optimized. The influence of phage incubation time on the modified electrode was investigated (Fig. S5). The results indicate an increase in inhibition of current response from 1 to 2 h due to nonconductive behavior of phages while analyzed at incubation interval of 30 min. There was a slight decrease in inhibition of current response while incubating phage for more than 2 h on the modified electrode, suggesting that the immobilized phages reached saturation at 2 h of incubation. The excess phages hinder electron transfer due to its nonconductive behavior. Hence, the incubation time of 2 h for phage immobilization on the modified electrode was chosen. The assessment of response time during a biosensor development is an important factor to be optimized. As this biosensor is based on the event of phage-induced cell lysis, hence the time taken by co-incubation of phage and bacteria till the bacterial cell lysis can decide the response time of the biosensor. Therefore, the developed phage-based electrode was incubated along with *Y. pseudotuberculosis* (7.00×10^6 CFU mL^{-1}) for 70 min, and the current response was investigated by DPV at interval of 10 min. As shown in Fig. S6, there was a slight decrease in current response at 0–20 min that is assigned to phage-induce bacterial capture and deposition on the electrode surface, thus hindering the electron transfer [23]. On the other hand, an apparent decrease in current response was observed at 30 min of incubation while no evident variation in current response was observed for the electrodes incubated at 40–70 min. Thus the optimal response time of the developed phage-based biosensor was recorded at incubation of 30 min where an obvious decrease in current response was observed. The results are in agreement with previously reported literature, claiming a sudden change in current response as a result of bacterial cell lysis, followed by release of progeny phages and cellular contents [46]. The electron/charge flow behavior between the medium and electrode is further explained by the released progeny phage particles that change the redox potential of the surrounding medium [47].

Our proposed PI–5–CA/rGO/AuNPs/phage-based biosensor was applied for detecting different cell density of *Y. pseudotuberculosis* under the optimum experimental conditions. The DPV responses were recorded in Fig. 5a. The other small peak around 0.03 V in DPV curves originates from the PI–5–CA, which is consistent with the previous report [20, 42,

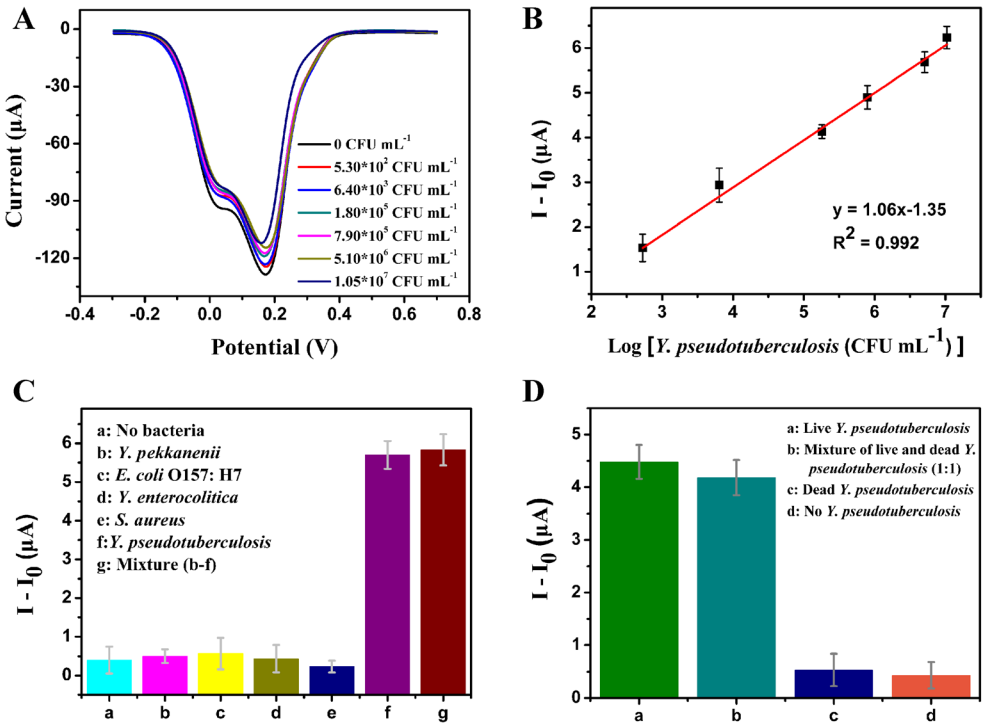

Fig. 5 The performance and specificity evaluation of our proposed PI–5–CA/rGO/AuNPs/phage-based biosensor for detection of *Y. pseudotuberculosis*. **a** DPV curves of the biosensor incubated with different cell density of *Y. pseudotuberculosis* at − 0.3~0.7 V in PBS (0.1 M, pH 6.0) (Ag/AgCl electrode as the reference electrode). **b** Linear relationship of current inhibition vs logarithmic of *Y. pseudotuberculosis* cell density. According to the DPV curves, I and I_0 are the peak currents of modified electrode before and after bacterial capture, respectively. **c** The detection specificity of the biosensor toward *Y. pseudotuberculosis* and other non-host bacteria at same concentration (3.00×10^6 CFU mL^{-1}). **d** DPV response of biosensor to live (3.30×10^5 CFU mL^{-1}), dead (3.30×10^5 CFU mL^{-1}), and mixture of live/dead *Y. pseudotuberculosis* (1:1). The standard deviation from the triplicate experiments is represented by error bars ($n = 3$)

48]. Along with increased cell density of *Y. pseudotuberculosis*, the peak current gradually decreased. This decrease in current response could be ascribed to the nonconductive behavior of *Y. pseudotuberculosis* captured by the immobilized phages. The more nonconductive *Y. pseudotuberculosis* was captured, the more obviously current signal changed. As shown in Fig. 5b, a good linear relationship of the current signal intensity was observed with the logarithm of *Y. pseudotuberculosis* cell density ranging from 5.30×10^2 to 1.05×10^7 CFU mL^{-1} (detailed data in the Supplementary Information file). This result indicates that the *Y. pseudotuberculosis* could be quantified by means of linear regression equation $y = 1.06x - 1.35$ with a linear correlation coefficient (R^2) of 0.992. The estimated LOD was to be 3 CFU mL^{-1} and calculated by the equation: LOD = 3 SD/k, where SD is the standard deviation of blank control ($n = 10$) while k is the slope of the linear regression equation.

The specificity of our proposed phage-based biosensor was evaluated by incubating the biosensor with some phage-non-host bacteria, including *Yersinia pekkanenii*, *E. coli* O157:H7, *Yersinia enterocolitica*, *S. aureus* at same cell density (3.00×10^6 CFU mL^{-1}). As represented in Fig. 5c, the current responses for these non-target bacteria are the same as the blank control. It is worth mentioning that the current response for the target *Y. pseudotuberculosis* is tenfold than other bacteria, indicating that the phage-based biosensor possesses a good selectivity in detecting *Y. pseudotuberculosis*. The excellent selectivity of our biosensor comes from phage as the recognition probe. The phages we isolated are highly specific to capture *Y. pseudotuberculosis* instead of other bacteria.

The discriminative detection of live bacterial cells is crucial as only living bacterial cells are regarded as pathogenic and considered a health risk. Thus, to evaluate the ability of our proposed biosensor to discriminate live cells in the mixture of live/dead bacterial cells, the current response was measured in the presence of different *Y. pseudotuberculosis* cells, i.e., live cells, dead cells, and the mixture of both live/dead cells (1:1). A small current response was observed for dead *Y. pseudotuberculosis* cells, which is similar to the current response for no bacteria. The obvious current response was observed for live *Y. pseudotuberculosis* cells, whereas an intervenient current response was observed for the mixture of live/dead cells (Fig. 5d). As a result of mixture, the concentration of live cells in the mixture solution decreased to half, so does the current response. Specifically, the current responses produced by living bacteria have reached nine times dead bacteria at the same concentration. It is obvious from the results that the phage-based biosensor is able to discriminate live *Y. pseudotuberculosis* cells in a mixture of live/dead cells.

Storage stability, reproducibility, and analysis in real samples

Storage stability and reproducibility are important considerations for sensors commercialization [49]. The storage stability of the phage-based biosensor was assessed within 4 weeks, stored at 4 °C and measured every week (Fig. S7). After 2 weeks and 4 weeks, the peak current of the biosensor decrease to 97.84% and 91.32% of its initial current respectively, indicating that this biosensor has acceptable long-term stability. In order to evaluate the reproducibility of the PI–5–CA/rGO/AuNPs/phage-based biosensor, the current responses were measured with *Y. pseudotuberculosis* (8.00×10^5 CFU mL^{-1}) by preparing seven separately modified electrodes and RSD was 3.5% (Fig. S8). The alteration of current responses indicates the phage-based biosensor is highly reproducible. In order to further estimate the practical application of the PI–5–CA/rGO/AuNPs/phage-based biosensor for *Y. pseudotuberculosis* detection, three river water samples were detected using our proposed biosensor and the plate count method. As displayed in Table 1, the recovery is from 95.41 to 104.05%, indicating acceptable reliability of the phage-based biosensor for real sample detection [33, 45].

Comparison with other reported methods

The performance of the phage-based biosensor has been evaluated by comparing it with previously reported methods for *Y. pseudotuberculosis* detection (Table 2). So far, there are not so many methods reported for *Y. pseudotuberculosis* detection, we collected almost all literatures for *Y. pseudotuberculosis* detection and listed in Table 2. Although ELISA and PCR-related methods are relative quick and reliable, they still suffer from some limitations, such as trained personnel, expensive

Table 1 Recovery tests for practical river water samples by phage-based biosensor and plate count

Sample No.	Spiked (CFU mL^{-1})	Detected (CFU mL^{-1})		Recovery (%)[a]	
		Present biosensor	Plate count	Present biosensor	Plate count
1	7.40×10^2	7.70×10^2	7.53×10^2	104.05	101.76
2	7.40×10^4	7.38×10^4	7.20×10^4	99.73	97.30
3	7.40×10^6	7.06×10^6	7.33×10^6	95.41	99.05

[a] Recovery (%) is expressed as the ratio of the number of detected/number of spiked

Table 2 The phage-based biosensor compared with other reported methods for *Y. pseudotuberculosis* detection

Methods	Recognition elements	Detection time	LOD	Sensitivity	Linearity region	Live/dead cells discrimination	Sample	Ref.
PCR assays	Nucleic acid-borne virulence genes	>2 h	N/A	N/A	N/A	No	–	[4]
Nested polymerase chain reaction (PCR)	DNA	>2 h	N/A	N/A	N/A	No	Feces	[50]
TaqMan-Based Real-Time PCR	*ail* gene	>18 h	28 CFU/10 g, 280 CFU/10 g	N/A	10^0–10^4	No	Carrots, beef	[51]
The real-time multiplex PCR assay	*wzz* gene	>3 h	100 fg DNA	1 cfu	N/A	No	Sputum and stool	[52]
Loop-Mediated Isothermal Amplification	16S–23S rDNA	>1 h	1 cfu/100 g	9.1 fg/μL	N/A	No	Milk powder	[53]
ELISA test	PsaA protein	>2.5 h	N/A	N/A	N/A	No	Blood plasma	[1]
Electrochemical biosensor	Phage vB_YepM_ZN18	~0.6 h	3 CFU mL^{-1}	N/A	5.30×10^2~1.05×10^7 CFU mL^{-1}	Yes	River water	Current work

N/A not applicable

reagents, unable to discriminate live/dead bacterial, and not applicable for on-site detection. Compared with other reported methods [1, 4, 50–53], the phage-based biosensor is more efficient with low limit of detection, short assay time, and able to discriminate live *Y. pseudotuberculosis* cells in mixture of live/dead cells. Further, the phage-based biosensor eliminated the need of complex sample pre-treatment steps such as bacterial culturing or concentration of nucleic acid. All these results demonstrated that the phage-based biosensor exhibited good analytical performance in *Y. pseudotuberculosis* detection.

Conclusion

In this work, a PI–5–CA/rGO/AuNPs/phage-based electrochemical biosensor was successfully developed for rapid and specific detection of *Y. pseudotuberculosis*. Thanks to the ultra-high redox stability and superior conductivity of the PI–5–CA/rGO/AuNPs materials, our biosensor performs well with a wide detection range, a low LOD, and assay time of 35 min. Moreover, the phage-based biosensor owns excellent stability and specificity, which is greatly favored for clinical analysis. Additionally, this biosensor reveals excellent storage stability and reproducibility, which is suitable for commercialization. The performance of the phage-based biosensor can be further improved by optimizing the density of phage immobilization. The developed PI–5–CA/rGO/AuNPs/phage-based electrochemical biosensor cannot be reused, but it is rapid, specific, sensitive, and low-cost, and is a promising tool for clinical applications of *Y. pseudotuberculosis* detection.

Supplementary Information The online version contains supplementary material available at https://doi.org/10.1007/s00604-020-04676-y.

Acknowledgments This work was supported by the National Key Research and Development Program of China under Grant 2017YFC1104402. The authors also thank the Analytical and Testing Center of Huazhong University of Science and Technology for SEM, EDX, Raman, TEM, and FTIR analyses.

Declarations

Conflict of interest The authors declare that they have no conflict of interest.

References

1. Wielkoszynski T, Moghaddam A, Bäckman A, Broden J, Piotrowski R, Mond-Paszek R, Kozarenko A, Ny T, Wilczynska M (2018) Novel diagnostic ELISA test for discrimination between infections with Yersinia enterocolitica and Yersinia pseudotuberculosis. Eur J Clin Microbiol Infect Dis 37:2301–2306. https://doi.org/10.1007/s10096-018-3373-9

2. Laukkanen R, Martínez PO, Siekkinen KM et al (2008) Transmission of Yersinia pseudotuberculosis in the pork production chain from farm to slaughterhouse. Appl Environ Microbiol 74:5444–5450. https://doi.org/10.1128/AEM.02664-07
3. Farooq U, Yang Q, Ullah MW, Wang S (2018) Bacterial biosensing : recent advances in phage-based bioassays and biosensors. Biosens Bioelectron 118:204–216. https://doi.org/10.1016/j.bios.2018.07.058
4. Thoerner P, Bin Kingombe CI, Wassenaar TM et al (2003) PCR detection of virulence genes in Yersinia enterocolitica and Yersinia pseudotuberculosis and investigation of virulence gene distribution. Appl Environ Microbiol 69:1810–1816. https://doi.org/10.1128/AEM.69.3.1810
5. Fukushima H, Tsunomori Y, Seki R (2003) Duplex real-time SYBR green PCR assays for detection of 17 species of food- or waterborne pathogens in stools. J Clin Microbiol 41:5134–5146. https://doi.org/10.1128/JCM.41.11.5134
6. Horisaka T, Fujita K, Iwata T, Nakadai A, Okatani AT, Horikita T, Taniguchi T, Honda E, Yokomizo Y, Hayashidani H (2004) Sensitive and specific detection of Yersinia pseudotuberculosis by loop-mediated isothermal amplification. J Clin Microbiol 42:5349–5352. https://doi.org/10.1128/JCM.42.11.5349
7. Richter Ł, Janczuk-Richter M, Niedziółka-Jönsson J, Paczesny J, Hołyst R (2018) Recent advances in bacteriophage-based methods for bacteria detection. Drug Discov Today 23:448–455. https://doi.org/10.1016/j.drudis.2017.11.007
8. Savas S, Altintas Z (2019) Graphene quantum dots as nanozymes for electrochemical sensing of yersinia enterocolitica in milk and human serum. Materials (Basel) 12:2189. https://doi.org/10.3390/ma12132189
9. Sobhan A, Lee J, Park MK, Oh JH (2019) Rapid detection of Yersinia enterocolitica using a single–walled carbon nanotube-based biosensor for Kimchi product. Lwt 108:48–54. https://doi.org/10.1016/j.lwt.2019.03.037
10. Walper SA, Lasarte Aragonés G, Sapsford KE, Brown CW III, Rowland CE, Breger JC, Medintz IL (2018) Detecting biothreat agents: from current diagnostics to developing sensor technologies. ACS Sensors 3:1894–2024. https://doi.org/10.1021/acssensors.8b00420
11. Justino CIL, Freitas AC, Pereira R, Duarte AC, Rocha Santos TAP (2015) Recent developments in recognition elements for chemical sensors and biosensors. TrAC - Trends Anal Chem 68:2–17. https://doi.org/10.1016/j.trac.2015.03.006
12. Singh A, Poshtiban S, Evoy S (2013) Recent advances in bacteriophage based biosensors for food-borne pathogen detection. Sensors (Switzerland) 13:1763–1786. https://doi.org/10.3390/s130201763
13. Rippa M, Castagna R, Pannico M, Musto P, Borriello G, Paradiso R, Galiero G, Bolletti Censi S, Zhou J, Zyss J, Petti L (2017) Octupolar metastructures for a highly sensitive, rapid, and reproducible phage-based detection of bacterial pathogens by surface-enhanced Raman scattering. ACS Sensors 2:947–954. https://doi.org/10.1021/acssensors.7b00195
14. Qiu JD, Liang RP, Wang R, Fan LX, Chen YW, Xia XH (2009) A label-free amperometric immunosensor based on biocompatible conductive redox chitosan-ferrocene/gold nanoparticles matrix. Biosens Bioelectron 25:852–857. https://doi.org/10.1016/j.bios.2009.08.048
15. Dong XX, Yang JY, Luo L, Zhang YF, Mao C, Sun YM, Lei HT, Shen YD, Beier RC, Xu ZL (2017) Portable amperometric immunosensor for histamine detection using Prussian blue-chitosan-gold nanoparticle nanocomposite films. Biosens Bioelectron 98:305–309. https://doi.org/10.1016/j.bios.2017.07.014
16. Zhang D, Fu L, Liao L, Liu N, Dai B, Zhang C (2012) Preparation, characterization, and application of electrochemically functional graphene nanocomposites by one-step liquid-phase exfoliation of natural flake graphite with methylene blue. Nano Res 5:875–887. https://doi.org/10.1007/s12274-012-0271-9
17. Kang D, Ricci F, White RJ, Plaxco KW (2016) Survey of redox-active moieties for application in multiplexed electrochemical biosensors. Anal Chem 88:10452–10458. https://doi.org/10.1021/acs.analchem.6b02376
18. Li X, Xia J, Zhang S (2008) Label-free detection of DNA hybridization based on poly(indole-5-carboxylic acid) conducting polymer. Anal Chim Acta 622:104–110. https://doi.org/10.1016/j.aca.2008.05.044
19. Zhang W (2016) Poly(indole-5-carboxylic acid)-functionalized ZnO nanocomposite for electrochemical DNA hybridization detection. J Solid State Electrochem 20:499–506. https://doi.org/10.1007/s10008-015-3071-9
20. Yang T, Ren X, Yang M, Li X, He K, Rao A, Wan Y, Yang H, Wang S, Luo Z (2019) A highly sensitive label-free electrochemical immunosensor based on poly(indole-5-carboxylicacid) with ultra-high redox stability. Biosens Bioelectron 141:111406. https://doi.org/10.1016/j.bios.2019.111406
21. Zhang T, Chen Y, Huang W, Wang Y, Hu X (2018) A novel AuNPs-doped COFs composite as electrochemical probe for chlorogenic acid detection with enhanced sensitivity and stability. Sensors Actuators B Chem 276:362–369. https://doi.org/10.1016/j.snb.2018.08.132
22. Santos MA (1991) An improved method for the small scale preparation of bacteriophage DNA based on phage precipitation by zinc chloride. Nucleic Acids Res 19:5442. https://doi.org/10.1093/nar/19.19.5442
23. Zhou Y, Marar A, Kner P, Ramasamy RP (2017) Charge-directed immobilization of bacteriophage on nanostructured electrode for whole-cell electrochemical biosensors. Anal Chem 89:5734–5741. https://doi.org/10.1021/acs.analchem.6b03751
24. Schwudke D, Ergin A, Michael K, Volkmar S, Appel B, Knabner D, Konietzny A, Strauch E (2008) Broad-host-range Yersinia phage PY100: genome sequence, proteome analysis of virions, and DNA packaging strategy. J Bacteriol 190:332–342. https://doi.org/10.1128/JB.01402-07
25. Rashid MH, Revazishvili T, Dean T, Butani A, Verratti K, Bishop-Lilly KA, Sozhamannan S, Sulakvelidze A, Rajanna C (2012) A Yersinia pestis-specific, lytic phage preparation significantly reduces viable Y. pestis on various hard surfaces experimentally contaminated with the bacterium. Bacteriophage 2:168–177. https://doi.org/10.4161/bact.22240
26. Hu Y, Hu D, Ming S, Duan X, Zhao F, Hou J, Xu J, Jiang F (2016) Synthesis of polyether-bridged bithiophenes and their electrochemical polymerization to electrochromic property. Electrochim Acta 189:64–73. https://doi.org/10.1016/j.electacta.2015.12.091
27. Ma X, Zhou W, Mo D, Hou J, Xu J (2015) Effect of substituent position on electrodeposition, morphology, and capacitance performance of polyindole bearing a carboxylic group. Electrochim Acta 176:1302–1312. https://doi.org/10.1016/j.electacta.2015.07.148
28. Liu H, Zhen S, Ming S, Lin K, Gu H, Zhao Y, Li Y, Lu B, Xu J (2016) Furan and pyridinechalcogenodiazole-based π-conjugated systems via a donor-acceptor approach. J Solid State Electrochem 20:2337–2349. https://doi.org/10.1007/s10008-016-3253-0
29. Gurunathan S, Han JW, Park JH, Kim JH (2014) A green chemistry approach for synthesizing biocompatible gold nanoparticles. Nanoscale Res Lett 9:1–11. https://doi.org/10.1186/1556-276X-9-248
30. Stankovich S, Dikin DA, Piner RD, Kohlhaas KA, Kleinhammes A, Jia Y, Wu Y, Nguyen SBT, Ruoff RS (2007) Synthesis of graphene-based nanosheets via chemical reduction of exfoliated graphite oxide. Carbon N Y 45:1558–1565. https://doi.org/10.1016/j.carbon.2007.02.034

31. Zhang J, Yang H, Shen G, Cheng P, Zhang J, Guo S (2010) Reduction of graphene oxide via L-ascorbic acid. Chem Commun 46:1112–1114. https://doi.org/10.1039/B917705A
32. Godipurge SS, Yallappa S, Biradar NJ, Biradar JS, Dhananjaya BL, Hegde G, Jagadish K, Hegde G (2016) A facile and green strategy for the synthesis of Au, Ag and Au–Ag alloy nanoparticles using aerial parts of R. hypocrateriformis extract and their biological evaluation. Enzym Microb Technol 95:174–184. https://doi.org/10.1016/j.enzmictec.2016.08.006
33. Li Y, Xie G, Qiu J, Zhou D, Gou D, Tao Y, Li Y, Chen H (2018) A new biosensor based on the recognition of phages and the signal amplification of organic-inorganic hybrid nanoflowers for discriminating and quantitating live pathogenic bacteria in urine. Sensors Actuators B Chem 258:803–812. https://doi.org/10.1016/j.snb.2017.11.155
34. Richter Ł, Bielec K, Leśniewski A, Łoś M, Paczesny J, Hołyst R (2017) Dense layer of bacteriophages ordered in alternating electric field and immobilized by surface chemical modification as sensing element for bacteria detection. ACS Appl Mater Interfaces 9:19622–19629. https://doi.org/10.1021/acsami.7b03497
35. Bhardwaj N, Bhardwaj SK, Mehta J, Mohanta GC, Deep A (2016) Bacteriophage immobilized graphene electrodes for impedimetric sensing of bacteria (Staphylococcus arlettae). Anal Biochem 505:18–25. https://doi.org/10.1016/j.ab.2016.04.008
36. Chauhan N, Narang J, Pundir CS (2011) Immobilization of rat brain acetylcholinesterase on ZnS and poly(indole-5-carboxylic acid) modified Au electrode for detection of organophosphorus insecticides. Biosens Bioelectron 29:82–88. https://doi.org/10.1016/j.bios.2011.07.070
37. Zhao D, Wang Y, Nie G (2016) Electrochemical immunosensor for the carcinoembryonic antigen based on a nanocomposite consisting of reduced graphene oxide, gold nanoparticles and poly(indole-6-carboxylic acid). Microchim Acta 183:2925–2932. https://doi.org/10.1007/s00604-016-1940-2
38. Liu X, Li WJ, Li L, Yang Y, Mao LG, Peng Z (2014) A label-free electrochemical immunosensor based on gold nanoparticles for direct detection of atrazine. Sensors Actuators B Chem 191:408–414. https://doi.org/10.1016/j.snb.2013.10.033
39. Miao X, Li Z, Zhu A, Feng Z, Tian J, Peng X (2016) Ultrasensitive electrochemical detection of protein tyrosine kinase-7 by gold nanoparticles and methylene blue assisted signal amplification. Biosens Bioelectron 83:39–44. https://doi.org/10.1016/j.bios.2016.04.032
40. Shan C, Yang H, Han D, Zhang Q, Ivaska A, Niu L (2010) Graphene/AuNPs/chitosan nanocomposites film for glucose biosensing. Biosens Bioelectron 25:1070–1074. https://doi.org/10.1016/j.bios.2009.09.024
41. Yang T, Gao Y, Liu Z, Xu J, Lu L, Yu Y (2017) Three-dimensional gold nanoparticles/prussian blue-poly(3,4-ethylenedioxythiophene) nanocomposite as novel redox matrix for label-free electrochemical immunoassay of carcinoembryonic antigen. Sensors Actuators B Chem 239:76–84. https://doi.org/10.1016/j.snb.2016.08.001
42. Talbi H, Billaud D, Louarn G, Pron A (2001) In-situ spectroscopic investigations of the redox behavior of poly (indole-5-carboxylic-acid) modified electrodes in acidic aqueous solutions. Spectrochim Acta Part A 57:423–433
43. Han L, Liu P, Petrenko VA, Liu AH (2016) A label-free electrochemical impedance cytosensor based on specific peptide-fused phage selected from landscape phage library. Sci Rep 6:1–10. https://doi.org/10.1038/srep22199
44. Moghtader F, Congur G, Zareie HM, Erdem A, Piskin E (2016) Impedimetric detection of pathogenic bacteria with bacteriophages using gold nanorod deposited graphite electrodes. RSC Adv 6:97832–97839. https://doi.org/10.1039/C6RA18884B
45. Zhang X, Xie G, Gou D, Luo P, Yao Y, Chen H (2019) A novel enzyme-free electrochemical biosensor for rapid detection of Pseudomonas aeruginosa based on high catalytic cu-ZrMOF and conductive super P. Biosens Bioelectron 142:111486. https://doi.org/10.1016/j.bios.2019.111486
46. Bhardwaj J, Devarakonda S, Kumar S, Jang J (2017) Development of a paper-based electrochemical immunosensor using an antibody-single walled carbon nanotubes bio-conjugate modified electrode for label-free detection of foodborne pathogens. Sensors Actuators B Chem 253:115–123. https://doi.org/10.1016/j.snb.2017.06.108
47. Wang D, Hinkley T, Chen J, Talbert JN, Nugen SR (2019) Phage based electrochemical detection of: Escherichia coli in drinking water using affinity reporter probes. Analyst 144:1345–1352. https://doi.org/10.1039/c8an01850b
48. Bartlett PN, Dawson DH, Farrington J (1992) Electrochemically polymerised films of 5-carboxyinodele. Preparation and properties. J Chem Soc Faraday Trans 88:2685–2695. https://doi.org/10.1039/FT9928802685
49. Mahato K, Srivastava A, Chandra P (2017) Paper based diagnostics for personalized health care: emerging technologies and commercial aspects. Biosens Bioelectron 96:246–259. https://doi.org/10.1016/j.bios.2017.05.001
50. Kageyama T, Ogasawara A, Fukuhara R, Narita Y, Miwa N, Kamanaka Y, Abe M, Kumazaki K, Maeda N, Suzuki J, Gotoh S, Matsubayashi K, Hashimoto C, Kato A, Matsubayashi N (2002) Yersinia pseudotuberculosis infection in breeding monkeys: detection and analysis of strain diversity by PCR. J Med Primatol 31:129–135. https://doi.org/10.1034/j.1600-0684.2002.01034.x
51. Thisted Lambertz S, Nilsson C, Hallanvuo S (2008) TaqMan-based real-time PCR method for detection of Yersinia pseudotuberculosis in food. Appl Environ Microbiol 74:6465–6469. https://doi.org/10.1128/AEM.01459-08
52. Matero P, Pasanen T, Laukkanen R et al (2009) Real-time multiplex PCR assay for detection of Yersinia pestis and Yersinia pseudotuberculosis. Apmis 117:34–44. https://doi.org/10.1111/j.1600-0463.2008.00013.x
53. Zhang H, Feng J, Xue R, du XJ, Lu X, Wang S (2014) Loop-mediated isothermal amplification assays for detecting yersinia pseudotuberculosis in milk powders. J Food Sci 79:967–971. https://doi.org/10.1111/1750-3841.12436